Published in final edited form as:
Radiat Res. 2009 May ; 171(5): 513–520. doi:10.1667/RR1658.1.

Propagation Distance of the α-Particle-Induced Bystander Effect: The Role of Nuclear Traversal and Gap Junction Communication

Sylvain Gaillard[a], **David Pusset**[a], **Sonia M. de Toledo**[b], **Michel Fromm**[a,1], and **Edouard I. Azzam**[b,1]

[a]Laboratoire de Chimie Physique et Rayonnements Alain Chambaudet, UMR CEA E4, Université de Franche-Comté, 25030 Besançon Cedex, France

[b]Department of Radiology, UMDNJ – New Jersey Medical School, Newark, New Jersey 07101

Abstract

When cell populations are exposed to low-dose α-particle radiation, a significant fraction of the cells will not be traversed by a radiation track. However, stressful effects occur in both irradiated and bystander cells in the population. Characterizing these effects, and investigating their underlying mechanism(s), is critical to understanding human health risks associated with exposure to α particles. To this end, confluent normal human fibroblast cultures were grown on polyethylene terephthalate foil grafted to an ultrathin solid-state nuclear track detector and exposed under non-perturbing conditions to low-fluence α particles from a broadbeam irradiator. Irradiated and affected bystander cells were localized with micrometer precision. The stress-responsive protein $p21^{Waf1}$ (also known as CDKN1A) was induced in bystander cells within a 100-μm radius from an irradiated cell. The mean propagation distance ranged from 20 to 40 μm around the intranuclear α-particle impact point, which corresponds to a set of ~30 cells. Nuclear traversal, induced DNA damage, and gap junction communication were critical contributors to propagation of this stressful effect The strategy described here may be ideal to investigate the size of radiation-affected target and the relative contribution of different cellular organelles to bystander effects induced by energetic particles, which is relevant to radioprotection and cancer radiotherapy.

INTRODUCTION

The health risks of human exposure to low-dose/low-fluence ionizing radiation remain unclear (1). Although human epidemiological studies are highly relevant to characterize these risks, they currently lack statistical power. Thus mechanistic studies have been proposed as a means to understand biological effects and to help evaluate the relationship between exposure to low-dose ionizing radiation and human health effects (1).

When exposed to low fluences from particulate radiations such as α particles, only some cells in a given population are traversed by a radiation track (2). However, the nonirradiated bystander cells may also be prone to stress as a result of molecular and biochemical signaling processes caused by direct or indirect communication between irradiated and bystander cells (3). Thus bystander effects can amplify the damage initiated by the targeted

[1]Address for correspondence: Department of Radiology, UMDNJ – New Jersey Medical School, 185 South Orange Avenue, MSB-F451, Newark, NJ 07101; e-mail: azzamei@umdnj.edu, or Laboratoire de Chimie Physique et Rayonnements Alain Chambaudet, UMR CEA E4, Université de Franche-Comté, 16, route de Gray, 25030 Besançon Cedex, France; e-mail: michel.fromm@univ-fcomte.fr.

effects of radiation, resulting in a non-linear dose-effect relationship (4,5). Cellular events induced by energy deposition from even a single α particle cause genetic changes, altered gene expression and lethality not only in traversed cells but also in neighboring bystander cells (6). These “non-targeted” stressful effects occur in cells of varying genetic background, lineage and organ origin (5,7,8).

Gap junction intercellular communication (GJIC), secreted diffusible factors and oxidative metabolism have been proposed as mediators of ionizing radiation-induced bystander effects (6,7). while most bystander effects were investigated *in vitro*, a few reports have shown that they can also be expressed *in vivo* (9–11). Therefore, bystander effects may affect human risk estimates of exposure to low-level ionizing radiation, in particular low fluences of high-linear energy transfer (LET) particulate radiations such as from radon gas in the home or galactic cosmic rays encountered during missions in space, which are extremely effective at inducing biological damage (12). During such exposures, only a small fraction of cells in an exposed tissue would be traversed by an energetic particle; however, the expression of bystander effects suggests that a greater fraction of cells may be at risk. In fact, it is estimated that 10–14% of lung cancer fatalities in the U.S. are linked to environmental radon and its α-particle-emitting decay products (13), and exposure to high-charge/high-energy particles is a major concern in long-term space flights (14). Thus determining the extent of propagation of radiation-induced bystander effects and the nature of the induced response is relevant not only to a basic understanding of the role of intercellular communication in the response to ionizing radiation but also in determining the size of the macroscopic target that is affected. These studies should help elucidate the mechanisms mediating bystander effects and reduce the uncertainty in estimating cancer risk from environmental exposures to low-fluence particulate radiations. They are likely to enhance our understanding of biological effects that result from non-uniform distribution of incorporated radioactivity such as α particles emitted from radionuclides used in therapeutic nuclear medicine or released during nuclear accidents or terrorist activities. They also offer avenues to characterize the nature of communicated signaling molecules and thus formulate strategies to protect normal tissue surrounding irradiated tumor targets.

Using targeted *microbeam* irradiation of artificial tissue, Belyakov *et al*. (15) showed that α-particle-induced bystander effects propagate up to 1 mm away from irradiated cells. The availability of low-cost, high-throughput, *broadbeam* α-particle irradiators, whereby large cell populations (millions of cells) are exposed rapidly to low fluences of energetic particles so that a small fraction of cells are hit, has greatly facilitated the study of radiation-induced bystander effects. Such irradiators permit investigation of sensitive biological end points under conditions where stress other than from irradiation is eliminated. However, this approach does not readily separate irradiated cells from bystander cells. Here we describe a physical/biological strategy that we have used effectively to colocalize, with micrometer accuracy, the impact of an α particle from a broadbeam irradiator with the structure of the hit cell without recourse to cellular perturbations that may affect induced biological responses. Using culture dishes whose base integrates a polyethylene terephthalate (PET) foil grafted to ultrathin CR-39, a solid-state nuclear track detector that enables optical microscopy tracking of hit cells, an etching procedure adapted to living media (16), and *in situ* detection of biological change, we have precisely identified irradiated and affected bystander cells in normal human fibroblast cultures exposed to low-fluence α particles. By merging pictures of induced changes in levels of $p21^{Waf1}$, a stress-responsive protein, with the precise cartography of α-particle traversals, we characterized the extent of propagation of biological changes in bystander cells by measuring the Euclidian distance distributions of responding cells relative to emitting ones. With relevance to understanding mechanisms underlying radiation-induced nontargeted effects, we show that α-particle nuclear traversal

and GJIC are critical contributors to the propagation of stressful bystander effects in normal human fibroblast cultures.

MATERIALS AND METHODS

Cell Culture

AG1522 normal human skin fibroblasts were from the Genetic Cell Repository at the Coriell Institute for Medical Research (Camden, NJ). Passage 10–11 cells were seeded at a density of ~1.5×10^5 cells in custom-made, 2.5μm-thick, PET-based dishes (internal diameter 2 cm) where the PET is UV-grafted to an ultrathin 10-μm CR-39 detector (16) and cultured as described (17). Cell cultures were irradiated when they were confluent (95–98% of cells in G_0/G_1). Control cells, referred to as external control, were sham-manipulated and handled in parallel with test cells.

Irradiation

Cell cultures were exposed at 37°C in an atmosphere of 95% air/5% CO_2 to α particles from a collimated ^{241}Am source at a dose rate of 2 cGy/min. Irradiation occurred from below, through the CR-39/PET base, with α particles of 3.2 MeV average energy (LET ~124 keV/μm) in contact with CR-39. The fraction of cells whose nucleus was traversed by an α particle was derived from Poisson statistics and estimates involving cell geometry, α-particle fluence and energy loss (18). for each irradiated dish, an area of the monolayer was masked during exposure to generate an internal control consisting of unirradiated cells.

Cell Movement

After irradiation, confluent cell cultures were incubated at 37°C in a 95% air/5% CO_2 atmosphere for 3 h prior to fixation for *in situ* detection of biological changes. During this time, cellular displacement must be evaluated to correlate α-particle trajectories with traversed cells with coherent accuracy. Thus cultures were monitored in real time during the 3-h period by confocal microscopy using a fixed high-magnification field. No cell movement was detected; hence the position of each track etched in CR-39 points precisely to an α-particle traversal through the monolayer.

Cell Fixation and Track Etching

At 3 h after exposure, cell cultures were rinsed in PBS^+ (PBS supplemented with 1 m*M* $MgCl_2$ and 0.1 m*M* $CaCl_2$) (pH 7.4) and fixed in 3% paraformaldehyde in PBS^+ (30 min). They were then rinsed (3×) and covered with 1 ml PBS^+ before etching latent tracks in CR-39 by immersing the base of the dishes in 10 *M* KOH solution at 37°C for 2 h (16). This procedure reveals small conical pits (diameter ~2 μm, depth ~1 μm) at the site of α-particle traversal and does not perturb the cells or their medium (16,19). After etching, the cultures were rinsed (3×) and incubated with fresh PBS^+; the CR-39 base was rinsed in pure water (3 ×, 5 min each) and dried in air.

In Situ Immunodetection

Cell monolayers were rinsed in 50 m*M* NH_4Cl (1×, 5 min) and PBS^+ (2×, 5 min each) and permeabilized in ice-cold 0.5% Triton X-100 buffer (50 m*M* NaCl, 3 m*M* $MgCl_2$, 200 m*M* sucrose, 10 m*M* Hepes at pH 7.4) (17). They were blocked in 1% BSA and reacted to anti-$p21^{Waf1}$ (EMD Biosciences, Inc.) or anti-53BP1 (Novus Biologicals, Inc.). After incubation with Alexa Fluor 488 goat anti-mouse IgG and Alexa Fluor 594 goat anti-rabbit IgG (Invitrogen), they were washed (5×) with PBS.

Microscopy

Device and setting—Samples were examined using a BioRad Radiance 2100™ scanning confocal microscope equipped with an argon laser (excitation at 488 nm). According to the two magnifications used (20× and 120×), respective numerical pictures were made of 1.2 × 1.2-μm^2 and 0.2 × 0.2-μm^2 pixels. To systematically discriminate the fluorescence signal from background noise and compare the fluorescence intensity among the cell cultures examined, the following was adopted: (1) Extrinsic parameters of the microscope were adjusted to eliminate a maximum of fluorescence signal in unirradiated cell cultures (external control), after which the microscope settings were fixed, (2) masked areas of partially irradiated cell cultures (internal control) were viewed to compare their fluorescence intensity with those recorded in external controls, and (3) different areas of coded irradiated cell cultures were examined. Etched tracks were viewed with the same microscope using visible light and high magnification (120×). Experiments were repeated at least three times.

Co-localization of tracks with cells overexpressing p21^{Waf1}—Hit cells within an exposed population were identified by mapping pictures of etched tracks with those of *in situ* p21^{Waf1} expression. However, the difference in size between etched tracks (few μm^2) and cell clusters (10^5 μm^2) does not permit direct superimposition of two pictures taken with a single magnification. Thus, for each cell cluster examined, a picture of p21^{waf1} induction was taken at low magnification (20×). The corresponding area was then revisited to identify etched tracks. For each track observed, pictures of the track and p21^{waf1}-overexpressing cells were taken at high magnification (120×). Traversed cells were identified by mapping pairs of corresponding pictures.

Image Treatment and Analysis

To localize α-particle traversals and responding cells, we pinpointed each in their respective picture using image analysis Software (AnalySiS by Olympus). Starting from an initial color picture, the picture elements (pixels) that belong to the objects of interest (etched track apertures, induced proteins) were isolated from all others using a color threshold. We then applied picture binarization, which consists of simple transformation of pixel values (0 for pixels out of the threshold and 1 for selected pixels). Last, we located all important picture elements by calculating relative Cartesian coordinates (x, y) of their center of gravity. In contrast to pictures of etched tracks, where tracks' openings appear as highly contrasted black circles with defined outlines, intracellular fluorescence pictures needed numerical treatment to improve an object's outline definition. Moreover, because pictures of etched tracks and responding cell clusters were taken using two different magnifications, they were co-localized by a three-stage procedure. Starting from pictures of tracks and cells over-expressing p21^{waf1} taken in the same field of view at 120× magnification (pixel size = 0.2 μm), we first calculated the relative position (ΔX_{Ti}, ΔY_{Ti}) between each etched track i (X_{Ti}, Y_{Ti}) and a reference fluorescent nucleus (X_N, Y_N) according to the following:

$$\Delta X_{Ti} = 0.2 \times (X_N - X_n)\,(\mu m) \quad (1)$$

$$\Delta Y_{Ti} = 0.2 \times (Y_N - Y_n)\,(\mu m) \quad (2)$$

Second, each responding cell within a cluster was located by determining the coordinates of intranuclear fluorescent spots in the low-magnification picture (pixel size 1.2 μm). The marked nucleus was then identified and the relative coordinates (x_N, y_N) were scored. Third,

the corresponding coordinates of each etched track (x_{Ti}, y_{Ti}) in the cluster were calculated as follows:

$$X_{Ti}=X_N-\frac{\Delta Y_{Ti}}{1.2}\ (\text{pixel}) \tag{3}$$

$$y_{Ti}=y_N-\frac{\Delta Y_{Ti}}{1.2}\ (\text{pixel}) \tag{4}$$

For each cluster of responding cells, these analyses and calculations yielded Cartesian coordinates of pixels corresponding to the relative positions of tracks and fluorescent spots in low-magnification (20×) pictures. These data were stored in two different coordinate matrices, each containing two columns (x, y) and a number of lines corresponding to the objects (tracks and fluorescent spots).

Fluorescence intensity—As a supplement to fluorescent spot location, the intensity of fluorescence was examined to compare the biological response within each cell in a cluster. Thus we implemented an image treatment to scale the intensity of fluorescence in false colors in the low-magnification pictures using Matlab® Software. Lowest intensities were painted in blue, higher intensities in green and greater intensities in red.

Distribution of Cell-Cell Signal Propagation Distances

To characterize the spread of bystander effects, we used confocal pictures of *in situ* $p21^{Waf1}$ induction in cultures exposed to 0 or 0.13 cGy. We developed a systematic procedure to evaluate the distribution of distances that separate an irradiated signal-emitting cell from its bystander signal-receiving cell in clusters of $p21^{Waf1}$-overexpressing cells. To achieve metrological data, we defined a precise model to describe signal propagation, applied a specific experimental protocol to identify signal-emitting cells within each cell cluster, and developed a computer code to automatically calculate relative distributions of signal propagation distances.

Theoretical model—We adopted the simplest model to characterize the spread of radial and isotropic stress signal(s) from a signal-emitting cell to its closest neighboring signal-receiving cell. If a cluster of responding cells contains more than one signal-emitting cell, each signal-receiving cell receives exclusively one signal from the nearest signal-emitting cell, and only the Euclidian distance between these two cells is considered. Conversely, the radiation-induced response in the signal-emitting cell is not considered in characterizing signal propagation. Signal emission is pinpointed precisely in the subcellular area where the α particle crosses the signal-emitting cell using position of the corresponding center of gravity of the etched track in the cell substrate. As for signal-receiving cell, the center of gravity of the cell nucleus (i.e., of the intracellular fluorescent spots) was used to locate signal reception.

Categorizing signal-emitting/receiving cells: the role of gap junctions—To identify signal-emitting cell within aggregated responding cells, the GJIC inhibitor 18-a-glycyrrhetinic acid (AGA) was added (50 μ*M* final concentration) to cell cultures 30 min before irradiation and remained for 3 h after exposure. Under this protocol, only traversed cells are expected to overexpress $p21^{Waf1}$ (17). The position of etched tracks under these responding cells would confirm α-particle traversal. To confirm inhibition of GJIC by AGA, the scrape-loading and dye transfer technique of El-Fouly *et al.* (20) was used.

Distribution of signal propagation distances—A Software in Visual Basic considers the two matrices relative to the position of tracks and intracellular fluorescent spots extracted from the analyzed pictures. Euclidian distances between track(s) and fluorescent spots are then calculated. For each spot, all distances are compared, and only the distance to the nearest track is considered. The software delimits a sector of influence for each track (graphically, each group of pixels constituting a sector is scaled as 256 gray levels depending on its distance to the track, from black to white when this distance increases). Then the cartography of fluorescent spots in the cluster is created (green circles centered on center of gravity of fluorescent spots) and merged on the track sector divided view. For each track, the nearest fluorescent spot corresponds to the biological response in irradiated signal-emitting cell. Thus, in each sector, we eliminated the shortest track-fluorescent spot distance before calculating signal propagation distances. Moreover, from a cluster to another, the number of signal-emitting cells may vary due to spatial non-uniformity of α-particle traversals. To obtain homogeneous and comparable results, the totality of distances calculated from a whole cluster was normalized to obtain a mean distribution of signal propagation distances around one track (i.e. one signal-emitting cell). For each sector, the longer a distance to one track (i.e. to one signal-emitting cell), the greater is the increase in the number of potential bystander cells. Thus, due to the quadratic behavior of such a radial expansion in a plane, a surface normalization was used. This quadratic behavior of the responding cell density as a function of the distance to the α-particle impact point is an important metrological constraint that must not be ignored. Finally, results for each cluster of responding cells are presented as a histogram giving the mean spatial density of signal-receiving cells (cells μm^{-2} $track^{-1}$) around one signal-emitting cell as a function of distance (in μm) between these communicating cells. These results correspond to a mean distribution of signal propagation distances around one signal-emitting cell. Then classical parameters of signal propagation were statistically extracted from calculated distributions: the mean distance of propagation ($\bar{d}$) and its relative standard deviation (σ); the longest distance of propagation (d_{max}) recorded in the cluster; and d_{66} and d_{95}, distances from which 66% and 95% of the total number of signal-receiving cells are respectively considered.

RESULTS

Qualitative and Quantitative Characteristics of the Bystander Effect: Up-regulation of $p21^{Waf1}$ in Confluent Human Fibroblast Cultures Exposed to a Very Low Fluence of α Particles

Several studies (17,21,22) have shown that $p21^{Waf1}$ is a sensitive marker for measuring radiation-induced bystander effects. The representative $p21^{Waf1}$ expression data in Fig. 1 confirm these studies and show that bystander effects are significantly expressed in density-inhibited AG1522 fibroblast cultures grown on PET/CR-39 dishes and exposed to a mean α-particle dose as low as 0.13 cGy. At this mean dose, ~0.9% of cell nuclei are traversed by a particle track (23). The *in situ* immunofluorescence data in Fig. 1C clearly show that more cells than predicted from nuclear irradiation respond to the exposure by up-regulating $p21^{Waf1}$, and the aggregate pattern of expression strongly suggests participation of neighboring bystander cells in the overall response. The data in Fig. 1A and B, respectively, show no up-regulation of $p21^{Waf1}$ in sham-irradiated cultures (external control) or in the masked area of irradiated cultures (internal control). The *in situ* data in Fig. 2A captured at lower magnification (20×) depict clusters of $p21^{Waf1}$-over-expressing cells within the exposed population. These typical results show that the spatial distribution of the propagated response is not homogeneous within a cell cluster. This suggests that, depending on their internal environment (e.g. redox environment), bystander cells may or may not up-regulate $p21^{Waf1}$; furthermore, induction and decay of the response may occur with variable kinetics in different cells.

To discriminate signal-emitting and signal-receiving cells in different clusters, we revisited cluster areas using higher magnification to localize signal-emitting cells (cells superimposed on black dots representing precise sites of α-particle traversals revealed by etching of CR-39 detector). The data in Figs. 2B and C illustrate the strategy used and highlight a typical example where two signal-emitting cells (cells 1 and 2) were identified within a cluster. Statistical data from the examined clusters are grouped in Table 1. These data show that at a mean dose of 0.13 cGy, each cluster of responding cells covers an area that has been crossed by a mean of six charged particles. By considering the ratio of the mean number of $p21^{Waf1}$-overexpressing cells and mean number of tracks within a cluster, ~ a threefold increase in $p21^{Waf1}$-expressing cells is obtained. When the mean numbers of tracks and signal-emitting cells within a cluster were considered, only 35% of α-particle traversals occurs through cell nuclei. Thus, by comparing the mean numbers of signal-emitting cells and signal-receiving cells within a cluster, an apparent increase of seven times in $p21^{Waf1}$-expressing cells is measured, indicating significant amplification of the biological response.

Scaling of $p21^{Waf1}$ intensities using false colors (Fig. 2D) shows that the biological response is variably expressed within cell clusters. Maximum induction of $p21^{Waf1}$ (colored in red) occurs in nuclei of cells crossed by an α particle. In contrast, $p21^{Waf1}$ induction in signal-receiving cells occurs with variable intensities (ranging from blue to red) and spatial distributions within nuclei.

Critical Impact Parameters to Generate a Signal Emitting Cell and Induce a Bystander Response: The Role of Gap Junction Communication and Nuclear Traversal

We have previously shown that GJIC has a major role in mediating α-particle-induced bystander effects (24)*; in situ* immunofluorescence studies in low-fluence-exposed cultures of human or rodent cells with compromised capacity to communicate through gap junctions showed that $p21^{Waf1}$ induction occurs in isolated cells only (17). However, in these studies where a broadbeam irradiation protocol was used, it was not possible to identify whether the isolated overexpressing cells are those that were traversed by a particle track. To identify cells with up-regulated $p21^{Waf1}$, we exposed confluent AG1522 cells grown in PET/CR-39 dishes to a mean dose of 0.13 cGy from α particles in the presence of a non-toxic concentration of the GJIC inhibitor AGA. Consistent with previous results (17), the *in situ* immunodetection data described in Fig. 3A reveal areas with only isolated nuclei that overexpress $p21^{Waf1}$. These representative areas correspond to a 9×10^4-μm^2 field of view. At 0.13 cGy, this area would be crossed by an average of five to six α particles. However, a mean of only one cell in this area up-regulated $p21^{Waf1}$. In contrast, parallel studies (Fig. 1 and Fig. 2) with cultures of GJIC-*competent* cells revealed greater numbers of cells up-regulating $p21^{Waf1}$ than those traversed by a particle track. Collectively, these results strongly support the involvement of gap junction communication in propagating α-particle-induced stressful effects to bystander cells. Moreover, with our PET/CR-39 dishes we show that cells up-regulating $p21^{Waf1}$ in exposed cultures of GJIC-inhibited cells are unequivocally those traversed by an α particle (Fig. 3B).

The difference between the number of tracks and responding cells illustrated in Fig. 3A indicates that α-particle cell traversals do not systematically result in $p21^{Waf1}$ up-regulation. To determine the effectiveness of α-particle traversal in $p21^{Waf1}$ induction, we mapped higher-magnification pictures of stained nuclei with corresponding pictures of tracks etched in CR-39 (Fig. 3B). Systematically, the isolated emitting cells were those whose nucleus had been crossed by an α particle. Merging pictures of 53BP1 expression, a DNA damage marker, and etched tracks, a spatial correlation between intensely fluorescent 53BP1 foci and α-particle traversals is noted (Fig. 3C). This impact parameter strongly suggests that $p21^{Waf1}$ induction results from DNA damage along the α-particle trajectory. These data thus support the concept that a signal-emitting cell is one that has been traversed by a particle

track, likely through the nucleus, where it causes DNA damage. Thus, when determining the metrology of propagation of α-particle-induced effects as shown below, only cells whose nuclei overhang an etched track are categorized as signal-emitting cells, whereas unirradiated $p21^{Waf1}$-responding cells are categorized as signal-receiving cells. Therefore, tracks that pinpoint traversed nuclei are considered below to establish the mean distance distributions separating a signal-receiving cell from its closest signal-emitting cell.

Lucifer yellow dye transfer data (Fig. 3D) confirmed that AGA inhibits functional GJIC, and Western blot analyses in AG1522 harvested at 3 h after exposure (Fig. 3E) confirmed those in Fig. 3A and indicated that $p21^{Waf1}$ is significantly up-regulated (3.6-fold) at doses as low as 0.1 cGy. This increase was prevented when cell cultures pre-incubated with AGA were exposed to low-fluence α particles.

Distribution of Signal Propagation Distances around Irradiated Cells

To illustrate metrological data obtained using our custom-made software (described in the Materials and Methods), a typical calculation based on the cluster picture in Fig. 2A is described in Fig. 4. After the two matrices relative to the tracks' positions and intranuclear $p21^{Waf1}$ fluorescent spots extracted from the analyzed pictures are loaded, software-generated cartography of $p21^{Waf1}$ overexpression (fluorescent green circles) is merged on the track sector(s) (Fig. 4A). For each track, the nearest fluorescent spot (corresponding to the irradiated nucleus within a signal-emitting cell) is eliminated (red crosses) before establishing the mean distribution of a signal propagation distances around a signal-emitting cell in the cluster studied. The corresponding chart depicting the relative distribution of signal propagation distances is presented in Fig. 4B. It represents the mean spatial density of a signal-receiving cell as a function of the Euclidian distance to an α-particle impact point (i.e., signal-emitting cell). In addition, the specific distances chosen to characterize signal propagation are displayed. In this example, the mean propagation distance of the bystander signal is ~37 ± 26 μm. The distances from which 66% and 95% of the total number of signal-receiving cells are considered are 64 and 76 μm, respectively, and the maximum distance of signal propagation is 95 μm. Statistical analyses of the clusters studied (Table 2) indicate that the mean propagation distance of the bystander effect revealed by $p21^{Waf1}$ overexpression ranges from 20 to 40 μm around the intranuclear α-particle impact point. Standard deviations relative to the mean signal propagation distance are typically between 50 and 100%. This value indicates that there is no preferential range of signal propagation distances and confirms the high non-uniformity of the signal-receiving cells' spatial distribution around signal-emitting cells. This may be due to differences in the spatial configuration of cells within confluent monolayers, which may vary among experiments due to variability in the arrangement, shape or orientation of the cells and the position of the nucleus therein. In addition, the biological end point studied occurred exclusively in the cell nucleus, whose center of gravity does not necessarily coincide with the center of gravity of the whole cell. Moreover, each cell within a cluster represents an individual living entity that may or may not develop the studied biological end point during the expression time investigated (3 h). Last, the maximal signal propagation distances were ~80 to 100 μm around α-particle impact points. Using a mean area of 800 μm^2 for an AG1522 fibroblast, this indicates that the induced biological response in a signal-emitting cell can potentially propagate within a region consisting of 30 surrounding cells.

DISCUSSION

The biological effects and health risks of low-dose ionizing radiation remain ambiguous and are the subject of intense debate. Characterizing these effects and elucidating their underlying mechanisms may guide human epidemiological analyses in areas where there is uncertainty. Together, mechanistic and epidemiological studies should contribute

significantly to the setting of adequate radiation protection guidelines. Using a strategy that combines the use of a broadbeam irradiator and tissue culture dishes fitted with a PET bottom grafted to a CR-39 SSNTD, we confirm (Fig. 1) that in confluent normal human fibroblast cultures exposed to low-dose α particles, a significantly greater number of cells than those actually hit are at risk of incurring stress (25). Importantly, we were able to precisely identify the irradiated and affected bystander cells in the population after exposure (Fig. 2). When gap junction communication was inhibited by incubating cell cultures with non-toxic concentrations of AGA, propagation of signaling processes leading to up regulation of $p21^{Waf1}$ in bystander cells was prevented (Fig. 3). Only cells whose nuclei were traversed by an α particle overexpressed $p21^{Waf1}$ and incurred DNA damage as reflected by 53BP1 foci (Fig. 3). These data are consistent with previous studies indicating that GJIC is critical in propagating radiation-induced effects that lead to modulation of gene expression and induction of DNA damage in bystander cells (24,26). They do not exclude the participation of other mechanisms such as secreted factors (27,28) and oxidative metabolism (29,30), but GJIC appears to be a major pathway for the bystander effect in confluent AG1522 human fibroblast cultures.

Using our software, which is based on the simplest model to describe signal propagation, we show that bystander effects can propagate within a 100-μm radius from a targeted cell, with non-targeted cells in proximity (within 20– 40 μm) to irradiated cells being most at risk (Fig. 4). This suggests that the area around a targeted cell that is likely to be affected by a bystander response, in terms of $p21^{Waf1}$ induction, corresponds to a set of ~30 cells. The 10-fold difference in the extent of propagation of the bystander effect between our studies and those reported (15) in artificial human tissue (100 μm and 1000 μm, respectively) may be due to cell type and tissue architecture. Competitive effects between propagated rescue and damage-signaling factors among irradiated and nonirradiated cells could also be involved. Our data (not shown) indicate that AG1522 cells express different connexin channels that propagate protective and stressful effects, respectively. It is likely that rescue effects communicated from bystander AG1522 cells are predominant as the distance from an irradiated cell increases. Refinement of our software by considering intrinsic parameters related to spatial distribution of cells within a population (cell shape and orientation, i.e. anisotropy) and to the cellular environment may help evaluate the extent of propagation of bystander effects.

Our studies have led to the important observation that nuclear traversal by an α particle has a major effect in propagating signaling events leading to up-regulation of $p21^{Waf1}$ in bystander AG1522 normal human fibroblasts (Fig. 2 and Fig. 3). Previous reports have indicated that in certain cell types, nuclear traversal is not a prerequisite to induce mutations or micronucleus formation in bystander cells. Using microbeam irradiation technology, a single helium-ion traversal through the cytoplasm of a cell, in a sparse culture, induced DNA damage in distant bystander cells (31,32). Furthermore, targeted cytoplasm irradiation induced nuclear mutations (33). Hence additional research is needed to elucidate the nature of the lesion that signals expression of the bystander effect in different cell types. It is likely that the differences between our results and those of others may emanate from differences in the redox environment of targeted cells. In fact, oxidative metabolism was shown to be a major factor mediating the expression of bystander effects (6,34). Altered cellular redox biochemistry resulting from reactive oxygen and nitrogen species (31,33) that are generated when radiation traverses the cytoplasm of certain cells may result in nuclear DNA damage in targeted cells, which signals expression of bystander effects. Whereas in our studies, confluent normal human diploid cells were exposed to α particles, tumor or transformed cells that have higher level of homeostatic oxidative stress were targeted by microbeam irradiation.

Characterizing bystander effects and elucidating their underlying mechanisms would affect not only our basic knowledge of intercellular communication in low-level ionizing radiation-exposed cell populations but would also have significant implications for radiation protection (4,35) and treatment of cancer by targeted radionuclide therapy (36,37). The use of our PET/CR-39 dishes in broadbeam or microbeam irradiation would permit targeting cellular/ subcellular regions under non-perturbing conditions, yet with fine precision to investigate sensitive end points that can expand our understanding of mechanisms underlying particulate radiation-induced bystander effects.

Acknowledgments

We thank Peter Carroll for microscopy support, Vincent Armbruster for performing Matlab® calculations, and Roger W. Howell for discussions. Grant CA92262-01 (EIA) from the NIH-National Cancer Institute supported this research.

REFERENCES

1. Health Risks from Exposure to Low Levels of Ionizing Radiation (BEIR VII). Washington, DC: National Academies Press; 2005. National Research Council, Committee to Assess Health Risks from Exposure to Low Levels of Ionizing Radiation.
2. Raju MR, Eisen Y, Carpenter S, Inkret WC. Radiobiology of α particles. III. Cell inactivation by α-particle traversals of the cell nucleus. Radiat. Res 1991;128:204–209. [PubMed: 1947017]
3. Little JB. Genomic instability and bystander effects: a historical perspective. Oncogene 2003;22:6978–6987. [PubMed: 14557801]
4. Brenner DJ, Little JB, Sachs RK. The bystander effect in radiation oncogenesis: II. A quantitative model. Radiat. Res 2001;155:402–408. [PubMed: 11182790]
5. Mothersill C, Seymour CB. Radiation-induced bystander effects—implications for cancer. Nat. Rev. Cancer 2004;4:158–164. [PubMed: 14964312]
6. Azzam EI, de Toledo SM, Little JB. Oxidative metabolism, gap junctions and the ionizing radiation-induced bystander effect. Oncogene 2003;22:7050–7057. [PubMed: 14557810]
7. Hamada N, Matsumoto H, Hara T, Kobayashi Y. Intercellular and intracellular signaling pathways mediating ionizing radiation-induced bystander effects. J. Radiat. Res. (Tokyo) 2007;48:87–95. [PubMed: 17327686]
8. Morgan WF. Non-targeted and delayed effects of exposure to ionizing radiation: II. Radiation-induced genomic instability and bystander effects *in vivo*, clastogenic factors and transgenerational effects. Radiat. Res 2003;159:581–596. [PubMed: 12710869]
9. Brooks AL, Retherford JC, McClellan RO. Effect of $^{239}PuO_2$ particle number and size on the frequency and distribution of chromosome aberrations in the liver of the Chinese hamster. Radiat. Res 1974;59:693–709. [PubMed: 4428016]
10. Watson GE, Lorimore SA, Macdonald DA, Wright EG. Chromosomal instability in unirradiated cells induced *in vivo* by a bystander effect of radiation. Cancer Res 2000;60:5608–5611. [PubMed: 11059747]
11. Xue LY, Butler NJ, Makrigiorgos GM, Adelstein SJ, Kassis AI. Bystander effect produced by radiolabeled tumor cells *in vivo*. Proc. Natl. Acad. Sci. USA 2002;99:13765–13770. [PubMed: 12368480]
12. Goodhead DT, Thacker J, Cox R. Effects of radiations of different qualities on cells: molecular mechanisms of damage and repair. Int. J. Radiat. Biol 1993;63:543–556. [PubMed: 8099101]
13. Health Effects of Exposure to Radon (BEIR VI). Washington, DC: National Academy Press; 1998. National Research Council, Committee on Health Risks of Exposure to Radon.
14. Cucinotta F, Durante M. Cancer risk from exposure to galactic cosmic rays: implications for space exploration by human beings. Lancet Oncol 2006;7:431–435. [PubMed: 16648048]
15. Belyakov OV, Mitchell SA, Parikh D, Randers-Pehrson G, Marino SA, Amundson SA, Geard CR, Brenner DJ. Biological effects in unirradiated human tissue induced by radiation damage up to 1 mm away. Proc. Natl. Acad. Sci. USA 2005;102:14203–14208. [PubMed: 16162670]

16. Gaillard S, Armbruster V, Hill MA, Gharbi T, Fromm M. Production and validation of CR-39-based dishes for alpha-particle radiobiological experiments. Radiat. Res 2005;163:343–350. [PubMed: 15733042]
17. Azzam EI, de Toledo SM, Little JB. Direct evidence for the participation of gap junction-mediated intercellular communication in the transmission of damage signals from alpha-particle irradiated to non-irradiated cells. Proc. Natl. Acad. Sci. USA 2001;98:473–478. [PubMed: 11149936]
18. Charlton DE, Sephton R. A relationship between microdosimetric spectra and cell survival for high-LET irradiation. Int. J. Radiat. Biol 1991;59:447–457. [PubMed: 1671694]
19. Gaillard S, Ross CJ, Ambruster V, Hill MA, Stevens DL, Gharbi T, Fromm M. Studies of UV-cured CR-39 recording properties in view of its applicability in radiobiological experiments with alpha particles. Radiat. Meas 2005;40:279–282.
20. El-Fouly MH, Trosko JE, Chang CC. Scrape-loading and dye transfer: A rapid and simple technique to study gap junctional intercellular communication. Exp. Cell Res 1987;168:422–430. [PubMed: 2433137]
21. Fournier C, Becker D, Winter M, Barberet P, Heiss M, Fischer B, Topsch J, Taucher-Scholz G. Cell cycle-related bystander responses are not increased with LET after heavy-ion irradiation. Radiat. Res 2007;167:194–206. [PubMed: 17390727]
22. Yang H, Asaad N, Held KD. Medium-mediated intercellular communication is involved in bystander responses of X-ray-irradiated normal human fibroblasts. Oncogene 2005;24:2096–2103. [PubMed: 15688009]
23. Neti PV, de Toledo SM, Perumal V, Azzam EI, Howell RW. A multi-port low-fluence alpha-particle irradiator: fabrication, testing and benchmark radiobiological studies. Radiat. Res 2004;161:732–738. [PubMed: 15161346]
24. Azzam EI, de Toledo SM, Gooding T, Little JB. Intercellular communication is involved in the bystander regulation of gene expression in human cells exposed to very low fluences of alpha particles. Radiat. Res 1998;150:497–504. [PubMed: 9806590]
25. Nagasawa H, Little JB. Induction of sister chromatid exchanges by extremely low doses of alpha-particles. Cancer Res 1992;52:6394–6396. [PubMed: 1423287]
26. Zhou H, Randers-Pehrson G, Waldren CA, Vannais D, Hall EJ, Hei TK. Induction of a bystander mutagenic effect of alpha particles in mammalian cells. Proc. Natl. Acad. Sci. USA 2000;97:2099–2104. [PubMed: 10681418]
27. Bowler DA, Moore SR, Macdonald DA, Smyth SH, Clapham P, Kadhim MA. Bystander-mediated genomic instability after high LET radiation in murine primary haemopoietic stem cells. Mutat. Res 2006;597:50–61. [PubMed: 16414086]
28. Mothersill C, Seymour C. Medium from irradiated human epithelial cells but not human fibroblasts reduces the clonogenic survival of unirradiated cells. Int. J. Radiat. Biol 1997;71:421–427. [PubMed: 9154145]
29. Azzam EI, de Toledo SM, Spitz DR, Little JB. Oxidative metabolism modulates signal transduction and micronucleus formation in bystander cells from alpha-particle-irradiated normal human fibroblast cultures. Cancer Res 2002;62:5436–5442. [PubMed: 12359750]
30. Bishayee A, Hill HZ, Stein D, Rao DV, Howell RW. Free-radical initiated and gap junction-mediated bystander effect due to nonuniform distribution of incorporated radioactivity in a three-dimensional tissue culture model. Radiat. Res 2001;155:335–344. [PubMed: 11175669]
31. Shao B, Folkard M, Michael BD, Prise KM. Targeted cytoplasmic irradiation induces bystander responses. Proc. Natl. Acad. Sci. USA 2004;101:13495–13500. [PubMed: 15345742]
32. Tartier L, Gilchrist S, Burdak-Rothkamm S, Folkard M, Prise KM. Cytoplasmic irradiation induces mitochondrial-dependent 53BP1 protein relocalization in irradiated and bystander cells. Cancer Res 2007;67:5872–5879. [PubMed: 17575156]
33. Wu LJ, Randers-Pehrson GR, Xu A, Waldren CA, Geard CR, Yu ZL, Hei TK. Targeted cytoplasmic irradiation with alpha particles induces mutations in mammalian cells. Proc. Natl. Acad. Sci. USA 1999;96:4959–4964. [PubMed: 10220401]
34. Bauer G. Low dose radiation and intercellular induction of apoptosis: potential implications for the control of oncogenesis. Int. J. Radiat. Biol 2007;83:873–888. [PubMed: 18058371]

35. Pollycove M, Feinendegen LE. Biologic responses to low doses of ionizing radiation: Detriment versus hormesis. Part 2. Dose responses of organisms. J. Nucl. Med 2001;42:26N–32N. 37N.

36. Boyd M, Ross SC, Dorrens J, Fullerton NE, Tan KW, Zalutsky MR, Mairs RJ. Radiation-induced biologic bystander effect elicited *in vitro* by targeted radiopharmaceuticals labeled with alpha-, beta-, and Auger electron-emitting radionuclides. J. Nucl. Med 2006;47:1007–1015. [PubMed: 16741311]

37. Kassis AI, Adelstein SJ. Radiobiologic principles in radionuclide therapy. J. Nucl. Med 2005;46 Suppl. 1:4S–12S. [PubMed: 15653646]

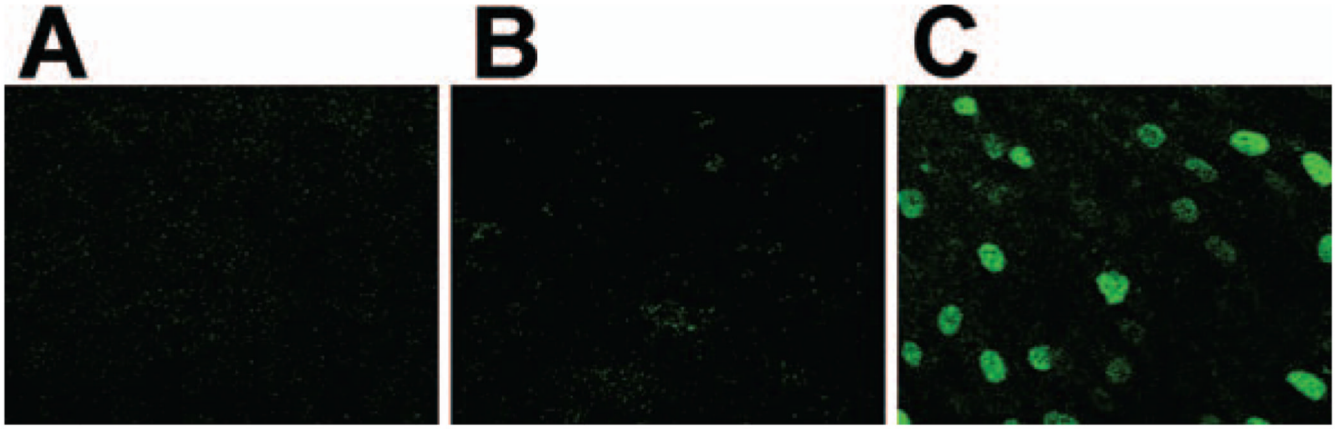

FIG. 1.

In situ immunofluorescence detection of $p21^{Waf1}$ in control and low-fluence α-particle-exposed cell cultures. Density-inhibited AG1522 fibroblasts cultures were exposed to 0.13 cGy and incubated at 37°C for 3 h. Panel A: Extinction of $p21^{Waf1}$ background fluorescence in sham-irradiated cultures (external control). Panel B: $p21^{Waf1}$ expression in masked area of a partially irradiated cell culture (internal control). Panel C: Induction of $p21^{Waf1}$ in cells in cultures exposed to 0.13 cGy (~1 cell in 100 is traversed through the nucleus at this mean dose).

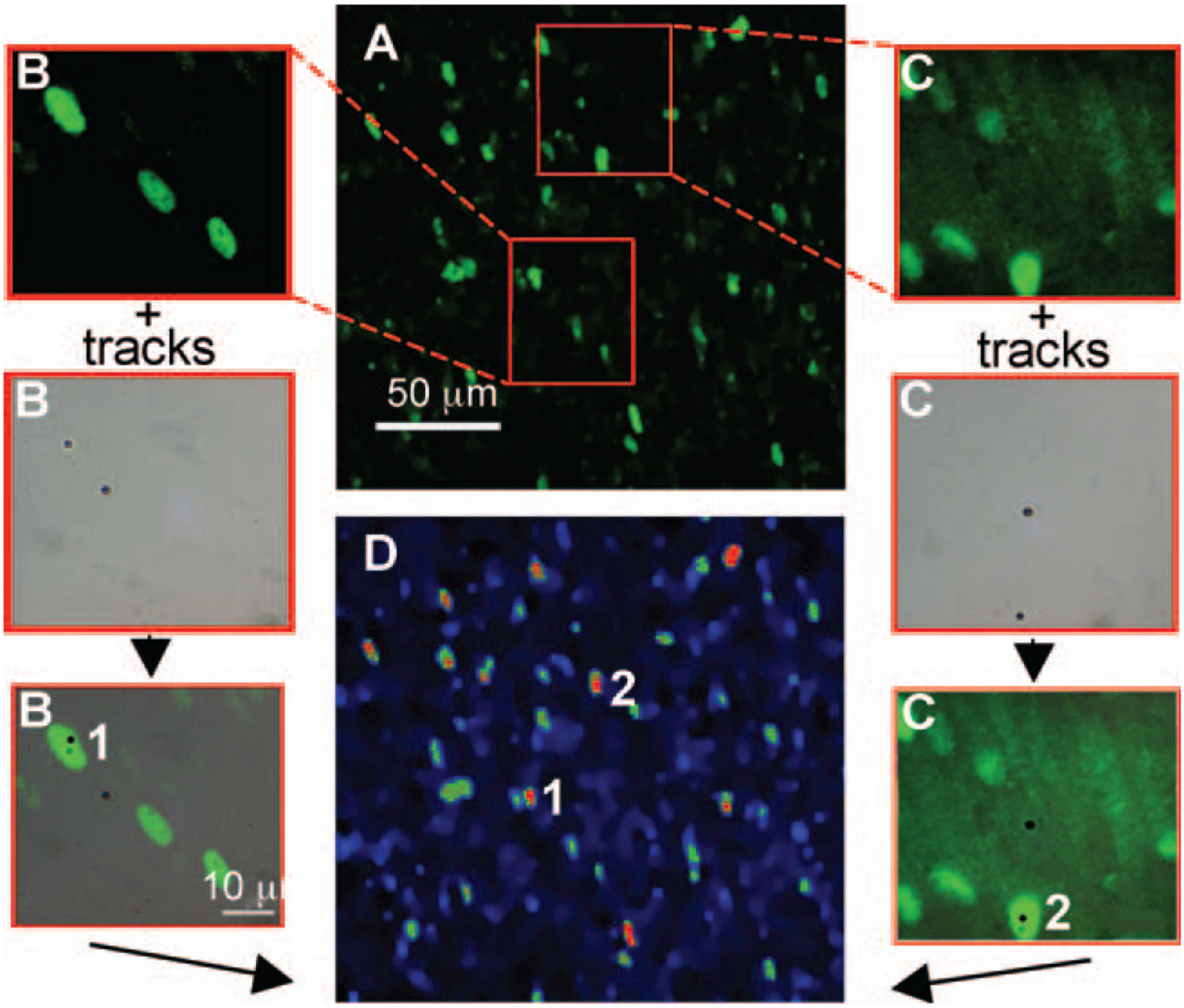

FIG. 2.

Correlation of the extent of $p21^{Waf1}$ induction with the number of α-particle track traversals. Confluent AG1522 fibroblast cultures grown on PET-CR-39 dishes were exposed to 0.13 cGy, incubated for 3 h at 37°C, and fixed with paraformaldehyde, and the CR-39 was etched in KOH. Panel A: Typical *in situ* immunofluorescence representation of $p21^{Waf1}$ up-regulation occurring in cell aggregates (original magnification 20×). Panels B and C: Illustration of the procedure used to locate irradiated nuclei or signal-emitting cells (numbered 1 and 2) within a cluster of responding cells. Panel D: False color illustration of $p21^{Waf1}$ overexpression scaled as a function of fluorescence intensity (from blue color for lower intensities to red color for higher intensity).

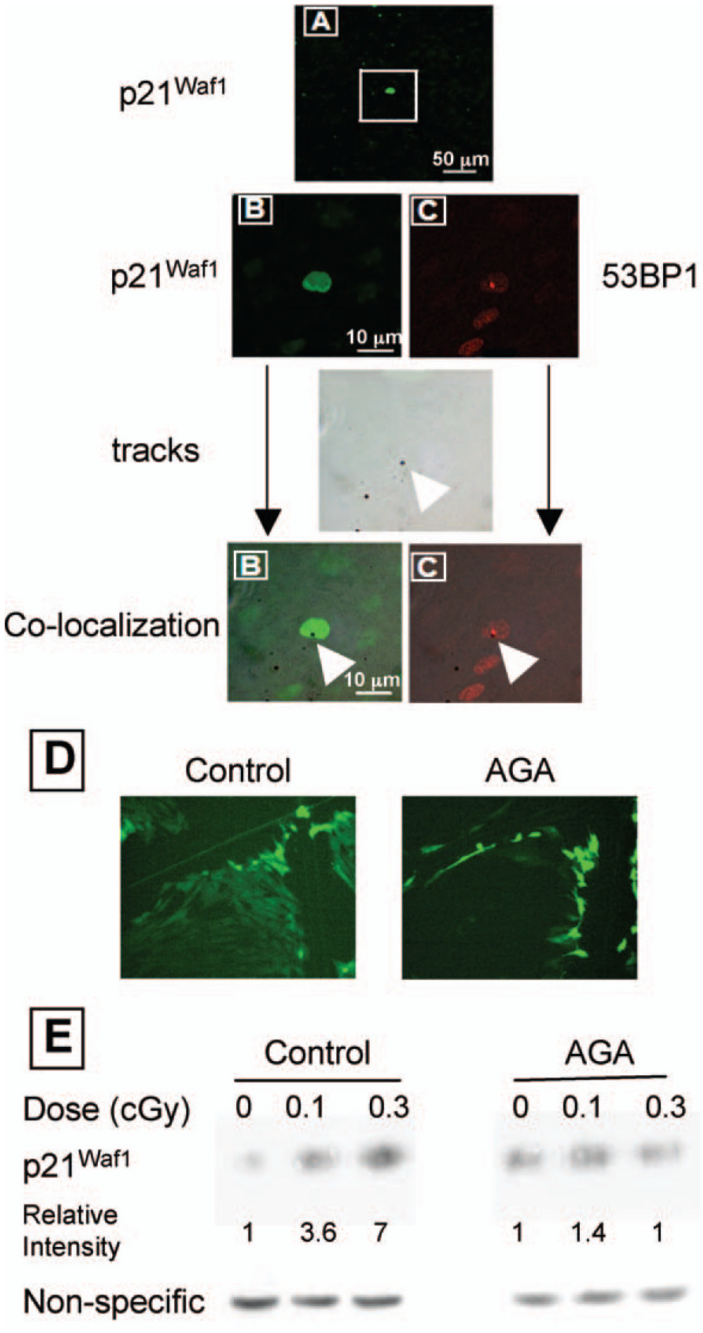

FIG. 3.

In situ expression of $p21^{Waf1}$ and 53BP1 in *confluent* AG1522 cell cultures at 3 h after exposure to α particles (0.13 cGy) in the presence of the gap junction inhibitor AGA (50 μ*M*). Panel A: Image (original magnification 20×) showing induction of $p21^{waf1}$ in isolated cells within exposed cultures. Panel B: Co-localization of intranuclear $p21^{Waf1}$ over-expression and etched tracks. Panel C: Co-localization of intranuclear 53BP1 induction and etched tracks. Panel D: Transfer of the fluorescent dye Lucifer yellow through gap junctions in AG1522 confluent, density-inhibited cultures (left panel) and inhibition of its transfer to adjacent cells by 50 μ*M* AGA (right panel). Panel E: Western blot analysis of $p21^{Waf1}$ expression in confluent AG1522 fibroblast cultures exposed to *α* particles in the absence or

presence of AGA (50 μ*M*). At a mean dose of 0.1 cGy, $p21^{Waf1}$ levels are increased by approximately threefold; this increase is not detected when cultures are irradiated in the presence of AGA.

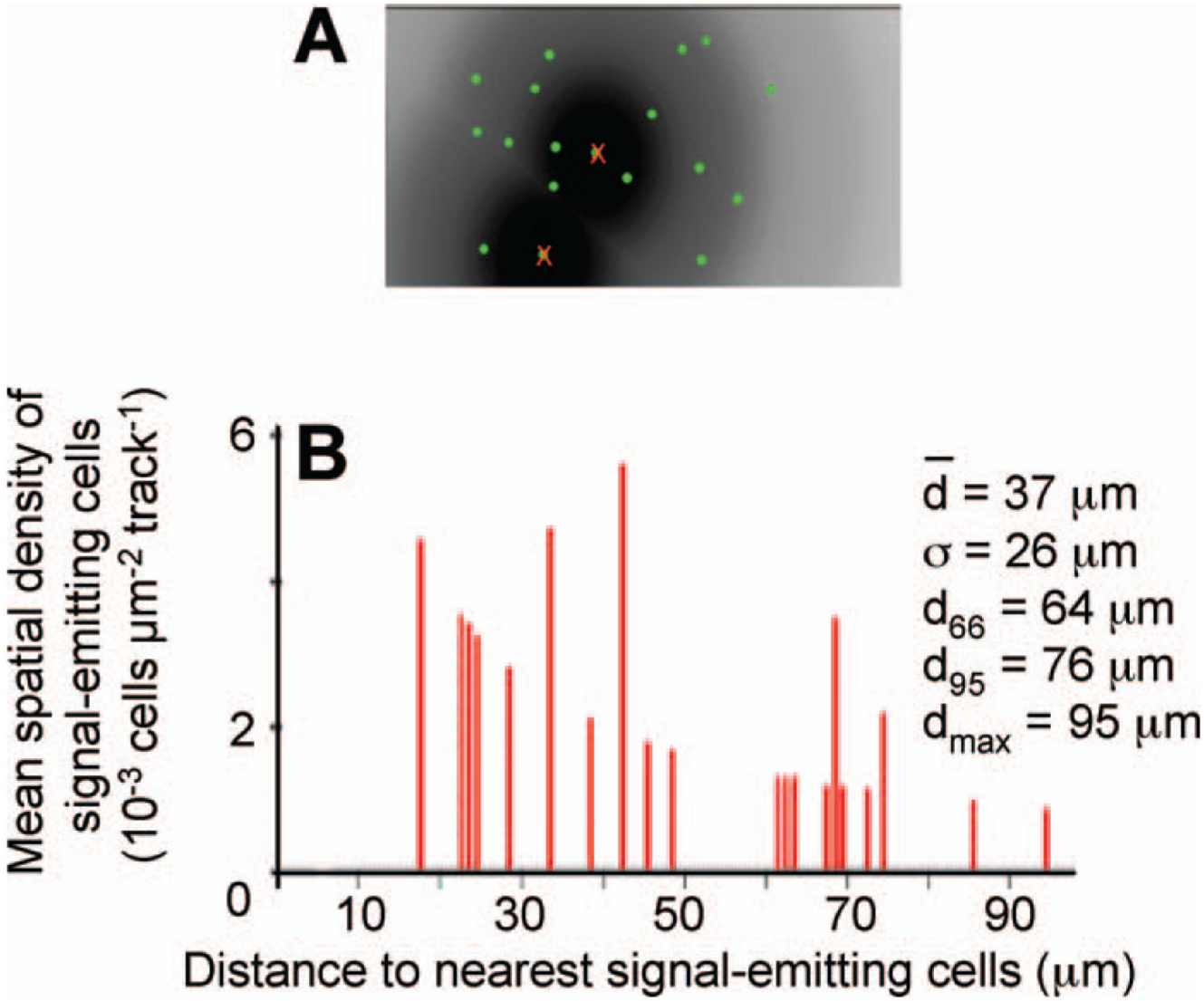

FIG. 4.

Panel A: Graphic interface of the Visual Basic software depicting spatial distribution of $p21^{Waf1}$ induction (green circles) merged on track (or signal-emitting cell) sectors of influence. For each track, the nearest fluorescence, corresponding to the radiation-induced response within signal-emitting cells is eliminated (red crosses) before calculating the mean distribution of signal propagation distances within a cell cluster. Panel B: Mean distribution of signal propagation distances in terms of the mean spatial density of signal-receiving cells as a function of distance to the nearest signal-emitting cell.

TABLE 1

Numbers of Tracks and Signal-Emitting or Receiving Cells within Typical Clusters of $p21^{Waf1}$-Overexpressing Cells in Confluent AG1522 Fibroblast Cultures Exposed to 0.13 cGy from ^{241}Am α. Particles

Signal-emitting cells ± SD	Signal-receiving cells ± SD	Tracks ± SD
2.3 ± 0.6	19.7 ± 8.1	6.3 ± 3.2

TABLE 2

Metrological Data for $p21^{Waf1}$-Responding Clusters: Signal Propagation Parameters in Cell Clusters

$\bar{d}$	σ_R	d_{66}	D_{95}	d_{max}
20–40 μm	50–100%	47–68 μm	63–74 μm	80–100 μm

Notes. $\bar{d}$ is the mean distance of propagation, σ_R its relative standard deviation; d_{66} and d_{95} are distances from which 66% and 95% of the total number of SRC are respectively considered, and d_{max} is the longest distance of propagation recorded in a typical cluster.